Engineering of the pH Optimum of *Bacillus cereus* β-Amylase: Conversion of the pH Optimum from a Bacterial Type to a Higher-Plant Type[†,‡]

Akira Hirata, Motoyasu Adachi, Shigeru Utsumi, and Bunzo Mikami*

Laboratory of Food Quality Design and Development, Graduate School of Agriculture, Kyoto University, Gokasho, Uji, Kyoto 611-0011, Japan

Received April 24, 2004; Revised Manuscript Received July 12, 2004

ABSTRACT: The optimum pH of *Bacillus cereus* β-amylase (BCB, pH 6.7) differs from that of soybean β-amylase (SBA, pH 5.4) due to the substitution of a few amino acid residues near the catalytic base residue (Glu 380 in SBA and Glu 367 in BCB). To explore the mechanism for controlling the optimum pH of β-amylase, five mutants of BCB (Y164E, Y164F, Y164H, Y164Q, and Y164Q/T47M/Y164E/T328N) were constructed and characterized with respect to enzymatic properties and X-ray structural crystal analysis. The optimum pH of the four single mutants shifted to 4.2−4.8, ∼2 pH units and ∼1 pH unit lower than those of BCB and SBA, respectively, and their k_{cat} values decreased to 41−3% of that of the wild-type enzyme. The X-ray crystal analysis of the enzyme−maltose complexes showed that Glu 367 of the wild type is surrounded by two water molecules (W1 and W2) that are not found in SBA. W1 is hydrogen-bonded to both side chains of Glu 367 and Tyr 164. The mutation of Tyr 164 to Glu and Phe resulted in the disruption of the hydrogen bond between Tyr 164 Oη and W1 and the introduction of two additional water molecules near position 164. In contrast, the triple mutant of BCB with a slightly decreased pH optimum at pH 6.0 has no water molecules (W1 and W2) around Glu 367. These results suggested that a water-mediated hydrogen bond network (Glu 367···W1···Tyr 164···Thr 328) is the primary requisite for the increased pH optimum of wild-type BCB. This strategy is completely different from that of SBA, in which a hydrogen bond network (Glu 380···Thr 340···Glu 178) reduces the optimum pH in a hydrophobic environment.

β-Amylase (α-1,4-glucan maltohydrolase, EC 3.2.1.2) catalyzes the liberation of β-anomeric maltose from the nonreducing ends of starch and glycogen. β-Amylase has been classified into family 14 of 93 glycoside hydrolase families [last updated February 19, 2004 (*1*, *2*)], and is present in higher plants and some bacteria (*3*, *4*). The three-dimensional structures of β-amylase from *Bacillus cereus* [BCB[1] (*5*, *6*)], soybean [SBA (*7*, *8*)], barley (*9*), and sweet potato (*10*) have already been determined. All of the previously determined structures of β-amylase exhibit a well-conserved active center in a cleft of the $(\alpha/\beta)_8$-barrel, although the exact barrel structure is different between higher-plant and bacterial β-amylase (Figure 1). Structural analysis of the β-amylase−maltose complex indicated that Glu 186 (Glu 172) and Glu 380 (Glu 367) in SBA (BCB) play important roles in the enzymatic reaction as a general acid catalyst and a general base catalyst, respectively (*5*−*7*). This finding is supported by the results of site-directed mutagenesis (*11*), affinity labeling (*12*, *13*), and the chemical rescue of the hydrolytic activity of the E367A mutant by azide (*14*). In terms of the different properties in the bacterial and higher-plant β-amylases, it has been reported that only bacterial β-amylases have the ability to bind and digest raw starch granules (*15*−*18*), which is mainly ascribed to the C-terminal starch-binding domain of bacterial enzymes and additionally to the starch-binding sites of the catalytic domain (Figure 1B). In addition to the raw starch digestive ability, differences were also found in the optimum pH, the specific activity, isoelectric points, and the number of sulfhydryl/disulfide groups (*19*). The optimum pH of bacterial β-amylase is ∼6.5−7.0, whereas that of higher-plant enzymes is

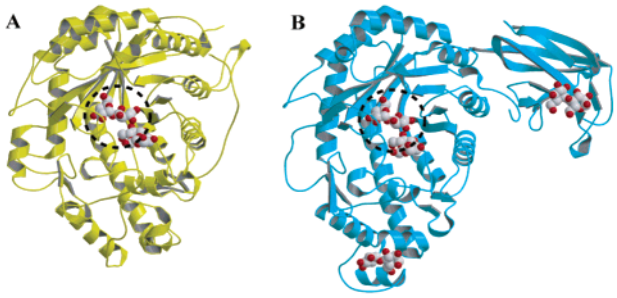

FIGURE 1: (A) X-ray crystal structure of the SBA−maltose complex (PDB entry 1Q6C, yellow). (B) X-ray crystal structure of the BCB−maltose complex (PDB entry 1BYZ, cyan). The two dashed circles indicate the structure around the active site. This figure was generated using MOLSCRIPT (*33*) and Raster3D (*34*).

[†] This work was supported, in part, by the National Project on Protein Structural and Functional Analysis from the Ministry of Education, Culture, Sports, Science and Technology to B.M. and S.U.

[‡] The atomic coordinates of the protein structure reported in this paper have been deposited in the Research Collaboratory for Structural Bioinformatics (RCSB) as entries 1VEM for BCB, 1VEN for Y164E, 1VEO for Y164F, and 1VEP for T47M/Y164E/T328N.

* To whom correspondence should be addressed. Telephone: 81-774-38-3763. Fax: 81-774-38-3764. E-mail: mikami@kais.kyoto-u.ac.jp.

[1] Abbreviations: BCB, *B. cereus* β-amylase; SBA, soybean β-amylase; SBD, starch binding domain.

10.1021/bi049173h CCC: $27.50
Published on Web 09/11/2004

~5.0−6.0. In a previous structural analysis of three mutants [M51T, E178Y, and N340T in SBA (*20*)], we demonstrated that a hydrogen bond network between the base catalyst (Glu 380) and adjacent side chains causes the lower pH optimum of SBA. The three residues around the base catalyst, Met 51, Glu 178, and Asn 340 in SBA and Thr 47, Tyr 164, and Thr 328 in BCB, are conserved in higher-plant and bacterial β-amylase, respectively. It has been suggested that this difference in architecture around the base catalyst between SBA and BCB contributes to the difference in the pH optimum of the respective enzymes. Therefore, it is hypothesized that the three residues in BCB regulate the higher pH optimum of BCB. To explore the mechanism for controlling the higher pH optimum of BCB, we focused on Tyr 164 and constructed four single mutants (Y164F, Y164E, Y164H, and Y164Q) having properties consistent with nonpolarity, negative charge, positive charge, and one triple mutant (T47M/Y164E/T328N), respectively.

MATERIALS AND METHODS

Construction of Mutant BCB Genes. Five mutants (Y164E, Y164F, Y164H, Y164Q, and T47M/Y164E/T328N) were generated using a QuikChange XL Site-Directed Mutagenesis Kit (Stratagene, La Jolla, CA) following the manufacturer's protocol. The PCR was performed in a total reaction volume of 50 μL containing 2.5 units of PfuTurbo DNA polymerase, 10× buffer, 200 μM dNTP, two synthesized mutagenesis primers (100 ng/mL each), and 5 ng/μL pBBCB as a template (pBluscript plasmid vector including the BCB gene). The two mutagenesis primers are complementary to opposite strands of the pBBCB (F and R denote the upstream and downstream primers, respectively): T47M-F, 5′-TTATGCTATTATGGTTGATTTTTG-3′; T47M-R, 5′-CAAAAATCAACCATAATAGCATAA-3′; Y164E-F, 5′-TGTAATTGCAAAAATAGAATTATCTGGAGGACCAG-3′; Y164E-R, 5′-CTGGTCCTCCAGATAATTCTATTTTTGCAATTACA-3′; Y164F-F, 5′-TGTAATTGCAAAAATATTCTTATCTGGAGGACCAG-3′; Y164F-R, 5′-CTGGTCCTCCAGATAAGAATATTTTTGCAATTACA-3′; Y164H-F, 5′-TGTAATTGCAAAAATACATTTATCTGGAGGACCAG-3′; Y164H-R, 5′-CTGGTCCTCCAGATAAATGTATTTTTGCAATTACA-3′; Y164Q-F, 5′-TGTAATTGCAAAAATACAATTATCTGGAGGACCAG-3′; Y164Q-R, 5′-CTGGTCCTCCAGATAATTGTATTTTTGCAATTACA-3′; T328N-F, 5′-CAAAGCTAGATGTAAATTTTACTTGCTTAG-3′; and T328N-R, 5′-CTAAGCAAGTAAAATTTACATCTAGCTTTG-3′.

The mutagenesis primers were extended using a thermal cycler (model 2400, Perkin-Elmer Life Sciences) for the PCR (14 cycles of denaturation for 30 s at 95 °C, annealing for 1 min at 57 °C, and elongation for 7 min at 68 °C). The PCR products were treated with 5 units of *Dpn*I at 37 °C for 1 h to digest the parental pBBCB template. The resultant vectors were transfected into *Escherichia coli* XL1-Blue supercompetent cells (Stratagene) using heat shock. The mutant DNA sequences were confirmed with a DNA sequencer.

Preparation of Mutant Proteins. For the construction of expression plasmids in *E. coli*, fragments from each of the five mutant genes were cut with *Xba*I and *Hin*dIII, and inserted between the *Xba*I and *Hin*dIII sites of expression vector pET21d (Novagen) to generate pEMutants. Mutants were expressed in *E. coli* strain HMS174 (DE3) harboring pEMutants. The cells were grown in TB medium without potassium phosphate buffer at 37 °C until the time of induction ($A_{600} = 0.8$) and cultured at 18 °C for 24 h. Protein expressions were induced by addition of isopropyl β-(−)-thiogalactopyranoside to a final concentration of 1.0 mM in *E. coli* strain HMS174 (DE3). The harvested cells were suspended in 50 mM sodium phosphate buffer (pH 7.0) containing 1 mM EDTA and 20 mM β-mercaptoethanol, and disrupted by sonication at 4 °C. The purification and activity assays of the BCB mutants were performed as described previously (*5*).

Enzyme Kinetics and pH Dependence of β-Amylase Activity. The values of k_{cat} and K_m for both BCB and its mutants were measured using potato amylopectin as a substrate (*21*). The concentrations of substrate were varied from $^1/_{10}$ of to 5 times the K_m value. In contrast to SBA, the activity−substrate concentration profile of BCB showed a cooperativity, and it was analyzed well by a Hill equation (eq 1) (*22*):

$$v = V_{max}[S]^n/K^n + [S]^n \quad (1)$$

where v is the initial rate, n is a qualitative indication of the level of cooperativity, K is the substrate concentration at which the velocity is half-maximal, and V_{max} is the maximum velocity. Calculations of V_{max} and K_m were performed with KaleidaGraph (Synergy Software). The substrate concentrations used for the determination of k_{cat} values are from 0 to ~3 times higher than the K_m values of the individual mutants. The Hill coefficient, n, was determined to be 1.6−2.0, indicating no significant difference among the mutants. The cooperativity found only in the BCB reaction is thought to be caused by the extra maltose binding sites of BCB (*5*).

The pH dependences of the k_{cat} activity of BCB and its mutants on potato amylopectin were determined at 37 °C in 0.05 M Britton-Robinson buffer or 0.025 M succinate buffer at pH 3.0−9.0. The ionic strength of the buffer solution at each pH was adjusted to 0.1 with NaCl. The apparent pK_1 and pK_2 values were calculated from the pH−k_{cat} profile with the KaleidaGraph nonlinear curve-fitting program using eq 2 (*23*):

$$(k_{cat})_{obs} = (k_{cat})_{max}/(1 + [H]/K_1 + K_2/[H]) \quad (2)$$

where $(k_{cat})_{obs}$ and $(k_{cat})_{max}$ are the maximum velocity (units M^{-1} s^{-1}) at each pH and pH-independent activity, respectively, [H] is the concentration of hydrogen ion, and K_1 and K_2 are dissociation constants of assumed catalytic groups of the enzyme−substrate complex. To reduce the uncertainty, we have limited the analysis of the kinetic parameter only for the changes in optimum pH and the dissociation constants of the assumed catalytic groups of the enzyme−substrate complexes.

Crystallization and Data Collection. On the basis of the crystallization condition in a previous report (*5*), crystallization of the wild type and T47M/Y164E/T328N were performed at 18 °C by the hanging drop vapor diffusion method, i.e., by mixing 5 μL of a 15 mg/mL protein solution in 0.05 M sodium acetate buffer with 5 μL of a mother liquid of 15% PEG6000, containing 5% saturated $(NH_4)_2SO_4$, and 0.1 M phosphate buffer (pH 6.5). The crystallizations of

Table 1: Data Collection and Refinement Statistics of BCB Mutants[a]

	wild type	Y164E	Y164F	T47M/Y164E/T328N
pH	6.5	4.6	4.6	6.5
space group	$P2_1$	$P2_1$	$P2_1$	$P2_1$
[maltose] (mM)	300	100	100	100
cell dimensions *a*, *b*, *c* (Å)	57.6, 92.8, 65.8	57.5, 92.9, 66.0	57.2, 92.2, 65.7	57.5, 92.7, 65.8
β (deg)	102.4	102.4	102.2	102.4
		Data Collection		
resolution range (Å)	27.93−1.72 (1.78−1.72)	30.49−1.87 (1.94−1.87)	29.24−1.88 (1.95−1.88)	35.71−1.84 (1.90−1.84)
no. of measured reflections	128372 (3995)	105686 (2257)	106234 (3114)	128668 (4166)
no. of unique reflections	63534 (3193)	48233 (1912)	49471 (2670)	53224 (2158)
R_{sym} (%)	4.2 (36.2)	8.8 (51.2)	9.1 (56.3)	8.9 (49.3)
completeness (%)	88.9 (44.8)	87.2 (34.6)	91.5 (50.0)	90.1 (36.7)
		Refinement		
resolution range (Å)	15−1.85 (1.92−1.85)	15−2.02 (2.09−2.02)	15−2.12 (2.20−2.12)	15−2.06 (2.13−2.06)
no. of reflections [$\sigma(F) > 0$]	49853 (3806)	37221 (2690)	33850 (2884)	36666 (3071)
no. of residues/waters	516/283	516/262	516/240	516/271
no. of maltoses (glucose)	−	4	3 (1)	3 (1)
no. of calciums	1	1	1	1
flexible loop (residues 92−99)	closed	closed	closed	closed
maltose-occupied sites	−2 to −1, +1 to +2	−2 to −1β	−2 to −1β	−2 to −1β, +1 to +2
alternate residues	329−333	16, 329−333	16, 330, 396	329−333
average *B*-factor (Å^2)	25.2	24.7	24.8	25.3
rmsd for bond lengths (Å)	0.005	0.006	0.006	0.006
rmsd for bond angles (deg)	1.26	1.25	1.27	1.27
R_{free} (%)	20.5 (29.2)	22.5 (35.5)	21.6 (33.4)	22.7 (36.9)
R-factor (%)	17.7 (27.8)	18.7 (32.4)	18.1 (31.0)	18.4 (33.3)

[a] The values in parentheses are those of the highest-resolution shell.

Table 2: Kinetic Parameters and pK_a Values for the Hydrolysis of Potato Amylopectin

		kinetic parameters			apparent pK_a values	
	optimum pH	apparent K_m (mg/mL)	k_{cat} (s^{-1})	% of wild-type value	pK_1	pK_2
wild type	6.7	0.73 ± 0.02	2739 ± 17.7	100	5.04 ± 0.10	8.53 ± 0.11
Y164E	4.6	1.24 ± 0.05	1129 ± 7.25	41	3.30 ± 0.05	5.92 ± 0.04
Y164F	4.8	0.92 ± 0.08	988 ± 24.55	36	3.56 ± 0.09	5.89 ± 0.06
Y164Q	4.2	1.22 ± 0.10	453 ± 15.78	17	3.18 ± 0.07	5.32 ± 0.05
Y164H	4.8	2.63 ± 0.21	92 ± 4.12	3	4.13 ± 0.04	5.64 ± 0.05
T47M/Y164E/T328N	6.0	0.47 ± 0.07	325 ± 12.2	12	4.23 ± 0.09	7.98 ± 0.09
SBA	5.4	1.90 ± 0.02	1280 ± 3.55	47	3.65 ± 0.11	8.07 ± 0.08

Y164E and Y164F were performed under the same conditions but using 0.1 M sodium acetate buffer (pH 4.6) in place of the phosphate buffer. The drops were left to equilibrate against 1 mL for 3 days, and then microseeding was performed using BCB crystals. Crystals appeared within 6 h of seeding and grew for 1 week. The wild-type and mutant BCB crystals used for data collection were approximately 1 mm × 0.5 mm × 0.5 mm in size. These crystals were all monoclinic and belonged to space group $P2_1$; the cell dimensions are given in Table 2. The wild type was soaked in the mother liquid containing 300 mM maltose for 30 min at 20 °C. In contrast, mutant crystals were cocrystallized with 100 mM maltose. These resulting crystals were mounted in thin-walled glass capillaries sealed with wax after addition of a small amount of mother liquor to one side. We avoided crystal freezing to prevent unexpected changes, such as a shift in pH. X-ray data of the wild-type and BCB mutant crystals were collected up to 1.72−1.88 Å resolution at room temperature using Cu Kα radiation (1.5418 Å) with a Bruker Hi-Star area detector coupled to a MAC Science M18XHF rotating anode generator, and the diffraction images were processed with the SADIE and SAINT software packages (Bruker).

Phasing and Refinement. The refined coordinates of BCB complexed with maltose (Protein Data Bank entry 1B9Z) were utilized as the initial model. The refinement program CNS (*24*) and the graphics program TURBO-FRODO (Architecture et Fonction des Maclomolécules Biologiques-CNRS, Paris, France) were used to refine and rebuild the BCB and the mutant models. The $2F_o - F_c$ and $F_o - F_c$ maps were used to locate the correct models. Several rounds of minimization and *B*-factor refinement, followed by manual model building, were carried out to improve the model. The structures were refined against all reflections from 15.0 Å to the highest resolution available without any $\sigma(F)$ cutoff (see Table 2). The R_{free} values of the wild type and BCB mutants were calculated for a randomly separated 10% of the data. The number of water molecules incorporated and the final refinement parameters are also given in Table 1. The stereo quality of the model was assessed using PROCHECK (*25*). The molecular structures of BCB, the mutants, and SBA were superimposed using a fitting program implemented in TURBO-FRODO.

RESULTS AND DISCUSSION

Effect of pH on Wild-Type and Mutant β-Amylase Activity. In this study, five mutants were all shown to have a decreased pH optimum, as shown in Figure 2. Table 2 shows the kinetic pK_a values estimated from the pH−activity profile and k_{cat} and K_m for hydrolysis of potato amylopectin at 37 °C at each

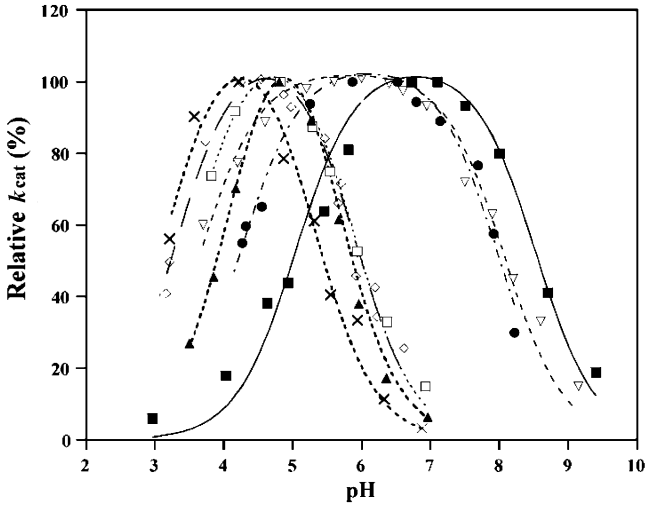

FIGURE 2: pH-dependent activity profiles of BCB (■), SBA (●), Y164E (□), Y164F (◇), Y164H (▲), Y164Q (×), and T47M/Y164E/T328N (▽). The lines show the fitting curve of the BCB, SBA, Y164 mutants, and triple mutant as calculated using eq 2.

optimum pH of the wild-type and mutant BCB together with SBA. The pH optima of Y164E, Y164F, Y164H, and Y164Q were dramatically shifted from the neutral region (pH 6.7) to the acidic region (pH 4.6, 4.8, 4.8, and 4.2, respectively) and were lower than that of SBA (pH 5.4). The shapes of their pH-dependent activity profiles were simple bell-shaped curves, and narrower than that of the wild type. The Y164E, Y164F, and Y164Q mutants exhibited decreased activities, with decreased k_{cat} values of 41, 36, and 17% of that of the wild-type enzyme, and increased apparent K_m values of 1.24, 0.92, and 1.22 mg/mL, respectively, which are 1.3−1.7 times higher than that of the wild-type enzyme (Table 2). The k_{cat} and K_m values of Y164H were less than 3% of and 3.6 times higher than those of the wild-type enzyme, respectively. The pH-dependent activity (k_{cat}) profiles are explained by the two kinetic pK_a values, pK_1 and pK_2. The pK_1 and pK_2 values of all mutants were ∼3.18−4.13 and ∼5.32−5.92, respectively, values which were lower than those of the wild-type enzyme (5.04 and 8.53, respectively). The decreased difference between pK_1 and pK_2 values reflects the narrow bell-shaped curve of all mutants. Despite the type of the mutated amino acid residues (Glu, Gln, Phe, and His), the pH optimum of the four single mutants decreased toward the acidic region, suggesting that the shift in the pH optimum is not caused by the electrostatic interaction between the catalytic residues and the mutated side chains at position 164. In contrast to the single mutants, the triple mutant (T47M/Y164E/T328N) had an optimum pH around pH 6.0, exhibiting broad bell-shaped curves as in the case of the wild type. Thus, the difference between pK_1 and pK_2 values of the triple mutant was compatible with that of the wild type, and this difference was smaller than those for the other mutants (Table 2). Kinetic analysis of the triple mutant showed that its k_{cat} value was 12% lower and its K_m value (0.47 mg/mL) was slightly lower than that of the wild-type enzyme. It should be noted that both changes in pK_1 and pK_2 contribute to the shift in the pH optimum of BCB mutants, in contrast to the changes in only pK_1 found in the mutants of SBA (*20*).

Structural Analysis. To investigate the structural changes required for the shifted pH optimum in BCB mutants, we determined the crystal structures of the wild type, two single mutants (Y164E and Y164F), and one triple mutant (T47M/Y164E/T328N) complexed with maltose at 1.85−2.12 Å resolution. The X-ray data collection and refinement statistics are summarized in Table 1. The crystallographic models for the wild type and for the Y164E, Y164F, and T47M/Y164E/T328N mutants were each refined to *R*-factors of <18.7% and to R_{free} values of <22.7%. From the Luzzati plots (*26*), the mean absolute positional errors were estimated to be 0.21−0.25 Å. A Ramachandran plot of the main chain conformation angles (*27*) showed that 86.9−88.4% of the residues lie within the core region, and 99.8−100% lie within the allowed region. With the exception of a short disordered main chain region (329−333) over the active site cleft, no significant changes occurred in the backbone structure between the wild-type enzyme and mutants. The root-mean-square (rms) deviations between the wild-type and mutant structures, calculated for all C_α atoms, were less than 0.19 Å. The flexible loop (residues 92−99), which plays an important role in the catalytic step, was in the closed form (Table 1). The $2F_o - F_c$ maps of the active site and the bound maltose were sufficiently clear to provide a reliable interpretation of the structural changes in the mutants with the exception of the glucose residue at the +1 site of Y164E and Y164F.

Structure of the Wild Type−Maltose Complex. Figure 3 shows the electron density map of the residues around Glu 367 and the two bound maltose molecules in wild-type BCB. The conformation of the glucose residue at subsite −1 in this structure of the wild type−maltose complex determined at pH 6.5 is slightly different from that determined at pH 4.6, as reported previously (*5*). This data set of the wild type−maltose complex could be refined by two maltose molecules at subsites −2 to −1 and +1 to +2, respectively, with a distorted sugar ring almost assuming the boat form with unknown anomer type at subsite −1. This conformation of the glucose residue at subsite −1 is almost the same as that of the wild-type SBA−maltose complex (*20*). It is suggested that the ratio of $^4C_1$ and the distorted glucose residue at subsite −1 depends on pH and that the distorted form becomes predominant at the optimum pH as reported for the SBA−maltose complex (*20*). The side chain of Glu 367 forms two direct hydrogen bonds with the side chains of Lys 287 and a glucose residue at subsite −1 [2.9 Å for the Glu 367 Oϵ2···Lys 287 Nζ distance and 2.6 Å for the Glu 367 Oϵ1···glucose (−1) O6 distance], as is the case of the wild-type SBA−maltose complex (20). In contrast to Glu 380 of the SBA−maltose complex, which forms one direct hydrogen bond with Asn 380, two water-mediated hydrogen bonds were identified at the side chain of Glu 367 of BCB [Glu 367 Oϵ2···W1···Tyr 164 Oη (2.4 and 2.8 Å) and Glu 367 Oϵ2···W2···Thr 47 Oγ1 (3.1 and 3.3 Å)] (Table 3). The hydrogen bond involving W1 forms a network with a hydrogen bond between Tyr 164 Oη and Thr 328 Oγ1 (2.5 Å). Thus, the three water-mediated hydrogen bonds seem to be responsible for the optimum pH of BCB being higher than that of SBA.

Structure of the Y164 Mutant−Maltose Complexes. In the case of the structure of Y164F (Figure 4A), the aromatic ring of Phe 164 could be flipped by rotating the χ_2 torsion angles approximately −79.5°. Two hydrogen bonds [Tyr 164 Oη···Thr 328 Oγ1 (2.5 Å) and Thr 47 Oγ1···W2 (3.3 Å)] (Table 3) found in the wild type were disrupted. Two novel

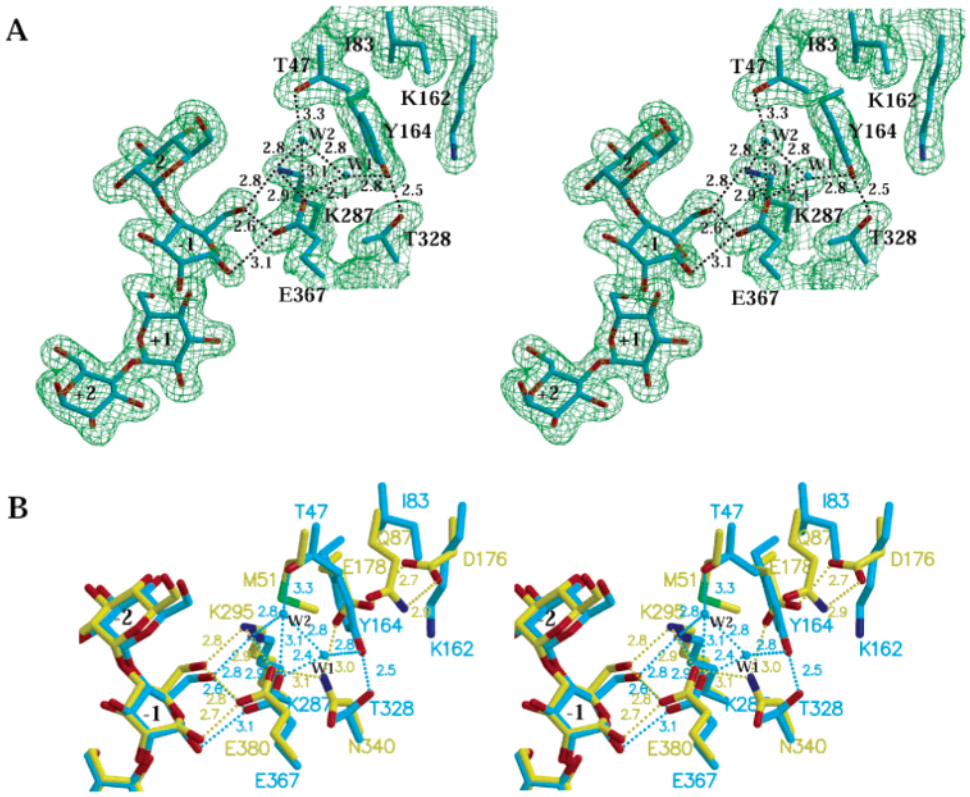

FIGURE 3: (A) Stereoviews of the structural conformation around Glu 367 of BCB (cyan) complexed with maltose. The electron density map (green, $2F_o - F_c$, contoured at 1.0σ) of the residues around the base catalyst and maltose are illustrated. (B) Stereodiagrams of the structural conformations around the base catalytic residue Glu 380 of SBA (yellow) complexed with maltose superimposed on the BCB (cyan) structure. The hydrogen bonds are represented by dotted lines. W1 and W2 denote water molecules This figure was generated using BOBSCRIPT (*35*), MOLSCRIPT (*33*), and Raster3D (*34*).

Table 3: Protein−Protein and Protein−Sugar Distances at the Active Site of Wild-Type and Mutant BCB[a]

		distance (Å)			
protein atom	protein (sugar) atom	wild type	Y164F	Y164E	T47M/Y164E/T328N
Thr 47 Oγ1	W2 O	3.3	3.7	4.2	−
Lys 162 Nζ	Glu 164 Oε2	−	−	2.9	3.2
Tyr 164 Oη	Thr 328 Oγ1	2.5	−	−	−
Tyr 164 Oη	W1 O	2.8	−	−	−
Glu 164 Oε1	Asn 328 Nδ2	−	−	−	3.2
Lys 287 Nζ	Glu 367 Oε2	2.9	3.0	3.4	3.2
Lys 287 Nζ	W2 O	2.8	2.6	2.6	−
Thr 328 Oγ1	W3 O	−	3.1	2.7	−
Glu 367 Oε1	CW O	−	2.9	3.0	3.3
Glu 367 Oε2	W1 O	2.4	2.3	2.8	−
Glu 367 Oε2	W2 O	3.1	2.7	2.4	−
W1 O	W2 O	2.8	2.8	2.6	−
W1 O	W3 O	−	2.8	2.8	−
W1 O	W4 O	−	3.3	2.6	−
W3 O	W4 O	−	3.3	3.4	−
Lys 287 Nζ	Glc −1 O6	2.8	2.9	2.8	3.0
Glu 367 Oε1	Glc −1 O6	2.6	3.3	3.3	3.2
Glu 367 Oε1	Glc −1 O1	3.1	−	−	−
CW O	Glc −1 O1	−	2.7	3.0	3.0

[a] W indicates a water molecule. CW indicates a catalytic water molecule.

water molecules (W3 and W4) were located at the vacated space of Cε and Oη of Tyr 164 in the wild type, allowing the formation of hydrogen bonds with W1 (2.7 and 2.9 Å), respectively. The binding mode of maltose in Y164F, in the active site, was different from that of the wild type. The glucose residue at subsite +1 was not found, possibly due to a high temperature factor of this glucose unit. The glucose residue at subsite −1 in Y164F took a β-anomeric $^4C_1$ conformation. Compared with that of the wild type, O1 of the glucose residue at subsite −1 in Y164F was shifted by 2.7 Å in the direction of the glucose residue at subsite +1. One water molecule was assigned as the catalytic water molecule, and it was found to be in almost the same position as that of O1 of the distorted glucose residue at subsite −1 in the wild-type BCB−maltose complex. Glu 367 in Y164F was perturbed and destabilized by the disruption of the water-mediated hydrogen bond (Glu 367···W1···Tyr 164). This may be ascribed to the decreased k_{cat} value compared with that of the wild type.

In the case of the structure of Y164E (Figure 4B), the substituted side chain of Glu 164 creates a hydrogen bond with Lys 162 at a distance of 2.9 Å (Table 3). Two novel water molecules (W3 and W4) occupied the same position of Y164F. W3 and W4 formed hydrogen bonds with W1 (2.8 and 2.9 Å, respectively). The binding mode of maltose in Y164E was also the same as that of Y164F, with an invisible glucose residue at subsite +1.

Structure of the Triple Mutant (T47M/Y164E/T328N)−Maltose Complex. In the structure of the triple mutant (Figure 4C), the substituted side chain of Met 47 excluded W1 and W2, resulting in the hydrophobic environment near Glu 367. Glu 164 created one hydrogen bond each with Asn 328 and Lys 162 (3.2 Å). The binding mode of maltose in the triple mutant was almost the same as that of the wild type, and a glucose residue at subsite −1 shifted toward subsite +1 as it did in the Y164 mutants. Although the glucose residue at

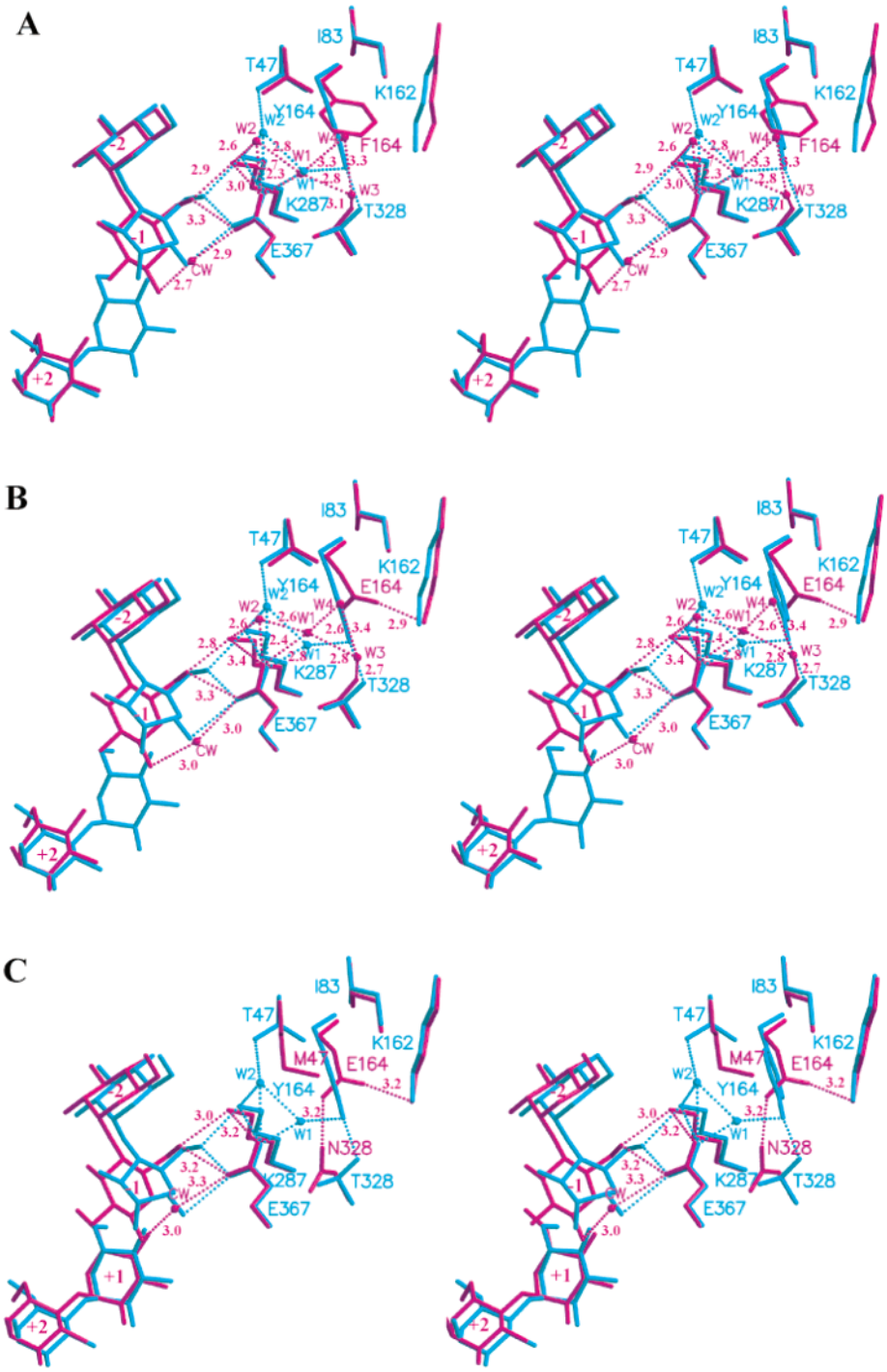

FIGURE 4: Stereoviews of the structural conformation around Glu 367 of BCB mutants (magenta) complexed with maltose superimposed on that of the wild-type (cyan) structure. The hydrogen bonds are represented by dotted lines. W denotes a water molecule. CW denotes a catalytic water molecule: (A) Y164F, (B) Y164E, and (C) T47M/Y164E/T328N. This figure was generated using MOLSCRIPT (*33*) and Raster3D (*34*).

subsite +1 was visible, the temperature factor of the glucose was still higher (64 Å^2) than that of the wild type (21 Å^2).

Structural Interpretation of the Decreased pH Optimum of BCB Mutants. In this study, we for the first time have succeeded in shifting the neutral pH optimum of BCB toward acidic pH. The optimum pH of the four single mutants shifted toward an acidic region much lower than that of SBA, irrespective of the kind of side chains (Glu, Gln, His, and Phe) at position 164. The crystal structure of the Y164E−maltose and Y164F−maltose complexes showed the deformation of three hydrogen bonds [that between W1 and Tyr 164, that between Tyr 164 and Thr 328, and that between Thr 47 and W2 (W1···Tyr 164 Oη···Thr 328 Oγ1 and Glu 367 Oϵ2···Thr 47 Oγ1)] and the occupation of two novel water molecules (W3 and W4) at the vacated space of Cϵ and Oη of Tyr 164 (Figure 4). The three hydrogen bonds (Glu 367 Oϵ2···W1, Glu 367 Oϵ2···W2, and W1···W2) of the wild type were maintained in the Y164 mutants (Table 3). The introduced W3 and W4 formed the novel hydrogen bonds with W1 instead of Tyr 164. These novel water−hydrogen bonds constituted the main structural difference between the wild type and the Y164 mutants (Table 3). The

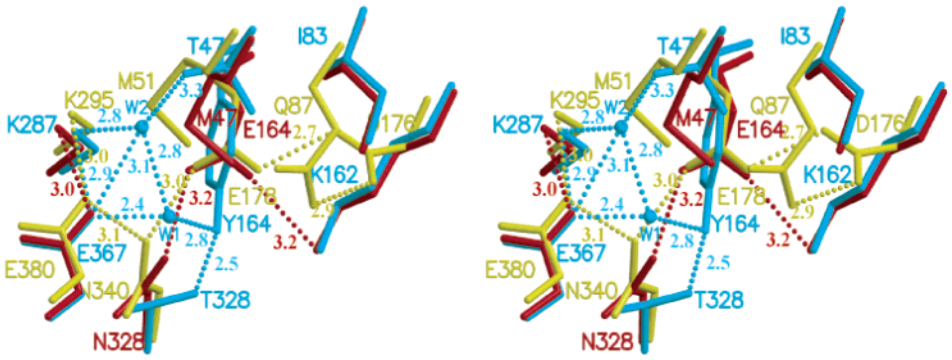

FIGURE 5: Stereoviews of the structural conformation around Glu 367 of T47M/Y164E/T328N (red) complexed with maltose superimposed on BCB (cyan) and SBA (yellow). The hydrogen bonds are represented by dotted lines. W denotes a water molecule. This figure was generated using MOLSCRIPT (*33*) and Raster3D (*34*).

kinetic pK_1 values of the single mutants (3.18−4.10) were compatible with the usual value of Glu in water (*28*), suggesting that the pK_1 of the wild type is increased by conformational factors. Though there is no direct evidence that the two kinetic pK values can be ascribed to those of the two catalytic carboxyl groups (Glu 367 and Glu 172), the following discussion is possible if we assume that the kinetic pK_1 represents the pK of Glu 367, as we did for the analysis of SBA mutants with increased pH (*20*). Hydrogen bonds can play a major role in modulating the pK_a values of dissociable side chains in proteins (*29*, *30*). In a previous study analyzing SBA mutants, we demonstrated that suitable hydrogen bond donors of side chains of Thr 340 in SBA can stabilize the negatively charged carboxyl group of Glu 380, resulting in a decreased pK_a of Glu 380 (*20*). In contrast, Fersht interpreted the increased pK_a of the carboxyl groups of lysozyme as follows. If a carboxyl group is in a region of relatively low polarity, its pK_a will be increased, since the anionic form is destabilized (*31*). The structural difference between the wild type and Y164 mutants in the active site of BCB suggests that W1, which is located between the side chains of Glu 367 and Tyr 164, is polarized after formation of a hydrogen bond with Tyr 164 Oη in the wild type. The polarization of W1 destabilizes the anionic form of Glu 367, resulting in an increase in the pK_a value of Glu 367 to approximately 5.0. Thus, the structures of Y164 mutants suggest that the decreased pH optimum is caused by the disruption of a hydrogen bond between W1 and Tyr 164 rather than by the electrostatic effect between Glu 367 and the mutated side chains at position 164. The disruption of the short hydrogen bond (Thr 328···Tyr 164, 2.5 Å) of Y164F resulted in a rotated aromatic ring of Phe 164 (Figure 4A), suggesting that the hydrogen bond fastened the side chain of Tyr 164 to a position in which Oη of Tyr 164 could form a hydrogen bond with W1. Thus, Thr 328 is also a key residue for regulation of the neutral pH optimum of BCB. It is assumed that Tyr 164 and Thr 328 act in concert to establish the pK_a values of Glu 367.

The structure of the triple mutant was superimposed onto that of BCB and SBA with rms deviations of 0.2 and 0.7 Å, respectively, as shown in Figure 5. Met 47 in the triple mutant, which corresponds to Met 51 of SBA, was shifted toward Ile 83 by 1.4 Å between Sδ of Met 47 of BCB and Sδ of Met 51 of SBA. Met 47 makes van der Waals contact with Ile 83, resulting in the formation of a hydrophobic environment near Glu 367. Glu 164 of the triple mutant was rotated by a χ^3 torsion angle of 32°, compared with Glu 178

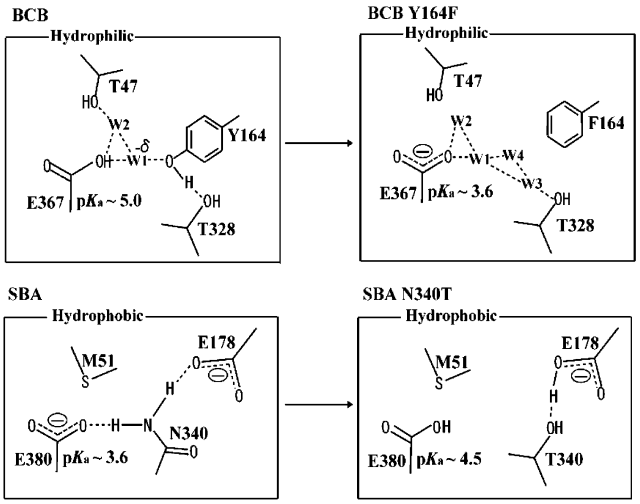

FIGURE 6: Difference in the strategies for pH optimum regulation in BCB and SBA.

of SBA, so that Oϵ2 of Glu 164 creates a hydrogen bond with Nζ of Lys 162 (3.2 Å). The side chain of Asn 328 faced the side chain of Glu 164 after a 33.5° rotation of the χ^2 torsion angle, forming a hydrogen bond between Oϵ1 of Glu 164 and Nδ2 of Asn 328 (3.2 Å). This may have been the cause of the deformation of the hydrogen bond between Oϵ2 of Glu 367 and Nδ2 of Asn 328, which was found in SBA (Oϵ2 of Glu 380 and Nδ2 of Asn 340, 3.1 Å). Since the pH−activity profile (pK_1 and pK_2) of the BCB triple mutant was almost the same as that of the SBA E178Y mutant (20), which has a disrupted hydrogen bond between Asn 340 and Glu 380 in SBA, the environment around Glu 367 of BCB was similar to that around Glu 380 of SBA. This suggests that Met 47 in BCB (Met 51 in SBA) is very important for the removal of W1 and W2, and makes the hydrophobic environment around Glu 367 (Glu 380). The finding that the pK_1 value of the triple mutant (4.2) was higher than that of the single mutant (3.18−4.1) may be ascribed to the change of the dielectric constant around Glu 367 (*32*).

We conclude that the mechanism of the different pH optima between SBA and BCB is as follows (Figure 6). Glu 367 of BCB, the base catalyst, is surrounded by a relatively more hydrophilic environment than SBA, because BCB has two water molecules (W1 and W2) at the active site. In the hydrophilic environment, two water-mediated hydrogen bonds (Glu 367···W2···Thr 47 and Glu 367···W1···Tyr 164···Thr 328) are formed by the three conserved residues (Thr

47, Tyr 164, and Thr 328). The polarization of W1 destabilizes the anionic form of Glu 367, resulting in the increase in the pK_a value of Glu 367 to 5.0. Therefore, the pH optimum of BCB is at neutral pH (6.7). In the case of Y164F and Y164E, the pK_a value of Glu 367 was 3.6, which is almost the same as that of carboxyl groups in a water solution (28). In contrast to BCB, Glu 380 of SBA is surrounded by a hydrophobic environment without any water molecules. In the hydrophobic environment, two hydrogen bonds (Glu 380···Asn 340···Glu 178), which are created by the three conserved residues (Met 51, Glu 178, and Asn 340), are formed. The hydrogen bond (Glu 380···Asn 340) stabilizes the anionic form of Glu 380, resulting in the observed decrease in the pK_a value of Glu 380 to 3.6. Therefore, the pH optimum of SBA is at acidic pH (5.4). In the case of the N340T mutant of SBA, the disruption of the hydrogen bond (Glu 380···Asn 340) caused the pK_a value of Glu 380 to be increased to 4.5. Consequently, BCB and SBA have different strategies for regulating their pH optima. BCB has a water-mediated hydrogen bond network (Glu 367···W1···Tyr 164···Thr 328) in a hydrophilic environment, which result in an increase in the pK_a value of Glu 367 from 3.6 (Y164F) to 5.0 (wild type) by destabilizing the deprotonated form of Glu 367, possibly due to the polarization of W1. In contrast to BCB, SBA has a hydrogen bond network (Glu 380···Asn 340···Glu 178) in a hydrophobic environment, which results in a decrease in the pK_a value of Glu 380 from 4.5 (N340T) to 3.6 (wild type) after stabilization of the deprotonated form of Glu 380.

ACKNOWLEDGMENT

Computation time was provided by the Supercomputer Laboratory, Institute for Chemical Research, Kyoto University, Kyoto, Japan.

REFERENCES

1. Henrissat, B. (1991) A classification of glycosyl hydrolases based on amino acid sequence similarities, *Biochem. J. 280*, 309−316.
2. Henrissat, B., and Romeu, A. (1995) Families, superfamilies and subfamilies of glycosyl hydrolases, *Biochem. J. 311*, 350−351.
3. Thoma, J. A., Sparadlin, E., and Dygert, S. (1971) Plant and animal amylases, *Enzymes (3rd Ed.) 5*, 115−189.
4. Nanmori, T. (1988) *Bacterial β-amylases: Handbook of Amylases and Related Enzymes*, Vol. 1, pp 94−99, Pergamon Press, Oxford, U.K. (edited by The Amylase Research Society of Japan).
5. Mikami, B., Adachi, M., Kage, T., Sarikaya, E., Nanmori, T., Shinke, R., and Utsumi, S. (1999) Structure of raw starch-digesting *Bacillus cereus* β-amylase complexed with maltose, *Biochemistry 38*, 7050−7061.
6. Oyama, T., Kusunoki, M., Kitamoto, Y., Takasaki, Y., and Nitta, Y. (1999) Crystal structure of β-amylase from *Bacillus cereus* var. mycoides at 2.2 Å resolution, *J. Biochem. 125*, 1120−1130.
7. Mikami, B., Hehre, J. A., Sato, M., Katsube, Y., Hirose, M., Morita, Y., and Sacchattini, J. C. (1993) The 2.0 Å resolution structure of soybean β-amylase complexed with α-cyclodextrin, *Biochemistry 32*, 6836−6845.
8. Mikami, B., Degano, M., Hehre, E. J., and Sacchattini, J. C. (1994) Crystal structures of soybean β-amylase reacted with β-maltose and maltal: active site components and their apparent roles in catalysis, *Biochemistry 33*, 7779−7787.
9. Mikami, B., Yoon, H.-J., and Yoshigi, N, (1999) The crystal structure of the sevenfold mutant of barley β-amylase with increased thermostability at 2.5 Å resolution, *J. Mol. Biol. 285*, 1235−1243.
10. Cheong, C.-G., Eom, S.-H., Chang, C., Shin, D.-H., Song, H.-K., Min, K., Moon, J.-H., Kim, K.-K., Hwang, K.-Y., and Suh, S.-W. (1995) Crystallization, molecular replacement solution, and refinement of tetrameric β-amylase from sweet potato, *Proteins 2*, 105−117.
11. Totsuka, A., and Fukawazawa, C. (1996) Functional analysis of Glu380 and Leu383 of soybean β-amylase. A proposed action mechanism, *Eur. J. Biochem. 240*, 655−659.
12. Nitta, Y., Isoda, Y., Toda, H., and Sakiyama, F. (1989) Identification of glutamic acid 186 affinity-labeled by 2,3-epoxypropyl α-D-glucopyranoside in soybean β-amylase, *J. Biochem. 100*, 1175−1183.
13. Oyama, T., Miyake, H., Kusunoki, M., and Nitta, Y. (2003) Crystal structures of β-amylase from *Bacillus cereus* var mycoides in complexes with substrate analogs and affinity-labeling reagents, *J. Biochem. 133*, 467−474.
14. Miyake, H., Otsuka, C., Nishimura, S., and Nitta, Y. (2002) Catalytic mechanism of β-amylase from *Bacillus cereus* var. mycoides: chemical rescue of hydrolytic activity for a catalytic site mutant (Glu367→Ala) by azide, *J. Biochem. 131*, 587−591.
15. Higashibara, M., and Okada, S. (1974) Studies on β-amylase of *Bacillus megaterium* strain no. 32, *Agric. Biol. Chem. 38*, 1023−1029.
16. Hoshino, M., Hirose, Y., Sano, K., and Mitsugi, K. (1975) Adsorption of microbial β-amylase on starch, *Agric. Biol. Chem. 39*, 2415−2416.
17. Saha, B. C., and Shen, G. J. (1987) Behavior of a novel thermostable β-amylase on raw starch, *Technology 9*, 598−601.
18. Ueda, S., and Marshall, J. (1980) Raw starch digestion by *Bacillus polymyxa* β-amylase, *Staerke 32*, 122−125.
19. Nomura, K., Yoneda, I., Nanmori, T., Shinke, R., Morita, Y., and Mikami, B. (1995) The role of SH and S−S groups in *Bacillus cereus* β-amylase, *J. Biochem. 118*, 1124−1130.
20. Hirata, A., Adachi, M., Sekine, A., Kang, Y.-N., Utsumi, S., and Mikami, B. (2004) Structural and enzymatic analysis of soybean β-amylase mutants with increased pH optimum, *J. Biol. Chem. 279*, 7287−7295.
21. Morita, Y., Aibara, S., Yamashita, H., Yagi, F., Suganuma, T., and Hiromi, K. (1975) Crystallization and preliminary X-ray investigation of soybean β-amylase, *J. Biochem. 77*, 343−351.
22. Atkinson, D. E. (1966) Regulation of enzyme activity, *Annu. Rev. Biochem. 35*, 85−123.
23. Dixon, M. (1953) The effect of pH on the affinities of enzymes for substrates and inhibitors, *Biochem. J. 55*, 161−170.
24. Brünger, A. T., Adams, P. D., Clore, G. M., DeLano, W. L., Gros, P., Grosse-Kunstleve, R. W., Jiamg, J.-S., Kuszewski, J., Nilges, M., Pannu, N. S., Read, R. J., Rice, L. M., Simonson, T., and Warren, G. L. (1998) Crystallography & NMR system: A new software suite for macromolecular structure determination, *Acta Crystallogr. D54*, 905−921.
25. Laskowski, R. A., MacArthur, M. W., Moss, D. S., and Thornton, J. M. (1993) *PROCHECK*: a program to check the stereochemical quality of protein structures, *J. Appl. Crystallogr. 26*, 283−291.
26. Luzzati, V. (1952) Traitement statistique des erreurs dans la determination des structures cristallines, *Acta Crystallogr. 5*, 802−810.
27. Ramakrishan, C., and Ramachandran, G. N. (1965) Stereochemical criteria for polypeptide and protein chain conformation, *Biophys. J. 5*, 909−933.
28. Forsyth, W. R., Antosiewicz, J. M., and Robertson, A. D. (2002) Empirical relationships between protein structure and carboxyl pK_a values in proteins, *Proteins 48*, 388−403.
29. Warshel, A. (1981) Electrostatic basis of structure−function correlation in proteins, *Acc. Chem. Res. 14*, 284−290.
30. Warshel, A., Russel, S. T., and Churg, A. K. (1984) Macroscopic models for studies of electrostatic interactions in proteins: limitations and applicability, *Proc. Natl. Acad. Sci. U.S.A. 81*, 4785−4789.
31. Fersht, A. (1999) Highly Perturbed pK_a's in Enzymes, in *Structure and Mechanism in Protein Science*, pp 188−189, W. H. Freeman and Co., New York.
32. Dwyer, J. J., Gittis, A. G., Karp, D. A., Lattman, E. E., Spencer, D. S., Stites, W. E., and Garcia-Moreno, B. (2000) High apparent dielectric constants in the interior of a protein reflect water penetration, *Biophys. J. 79*, 1610−1620.

33. Kraulis, P. J. (1991) *MOLSCRIPT*: a program to produce both detailed and schematic plots of protein structures, *J. Appl. Crystallogr. 24*, 946−950.
34. Merrit, E. A., and Murphy, M. E. P. (1994) *Raster*3*D* Version 2.0. A program for photorealistic molecular graphics, *Acta Crystallogr. D50*, 869−873.
35. Esnouf, R. M. (1997) An extensively modified version of MolScript that includes greatly enhanced coloring capabilities, *J. Mol. Graphics 15*, 132−134.

BI049173H